A Novel Dual-Band, Dual-Polarized, Miniaturized and Low-Profile Base Station Antenna

Yejun He, *Senior Member, IEEE*, Zhengzheng Pan, Xudong Cheng, Yuan He, Jian Qiao, and Manos M. Tentzeris, *Fellow, IEEE*

***Abstract*—In this paper, a novel dual-band, dual-polarized, miniaturized and low-profile base station antenna operating in the frequency bands of 820–960 and 1710–2170 MHz is designed. Elements are arranged such that high-frequency elements are embedded in low frequency elements to reduce volume. A baffle is used to reflect the transmitted power density in the forward direction and also improve isolation between elements. Therefore, surrounding isolation baffles and rectangular baffles are appended around high-frequency elements and low-frequency elements, respectively. The diameter of the proposed antenna cover is only 200 mm, which is smaller than the existing antenna diameter of 280 mm. Compared with the other commonly used antennas, the proposed antenna also has some advantages such as concealment and low profile using a tubular form of radome, which can easily integrate the proposed antenna with the surrounding environment. The measured results verify that the proposed antenna meets the stringent design requirements: voltage standing wave ratio (VSWR) is less than 1.3, the isolation is greater than 30 dB, and the pattern parameters also meet telecommunications industry standards.**

***Index Terms*—Base station antenna, dual-band, dual-polarized, miniaturized and low-profile antenna.**

I. Introduction

ONE of the key components in wireless mobile communication systems is the base station antenna, which plays a critical role in converting the electromagnetic waves that propagate in free space to electric current in the base station's circuitry [1]–[4]. With the development of various generations of wireless mobile communication systems [5], antennas have achieved numerous milestones for different standards, such as advanced mobile phone service (AMPS) system [6], 2G base station antenna for GSM and CDMA system [7], 3G base station antenna for TD-SCDMA, WCDMA, CDMA2000, and Wimax system [8], [9], [10] as well as 4G (LTE/LTE-Advanced) base station antenna [11], [12]. In addition, most of related work on base station antenna design focuses on the miniaturization, broadband and dual frequency band [13]–[15], and smart antenna [9] characteristics.

As more mobile users are involved in wireless networks, the systems require an ever increasing capacity and more base station antennas. To optimize the resource utilization efficiency of the base station antennas, 5G/4G/3G systems are established on top of existing 4G/3G/2G systems to enable multiple systems to simultaneously cover the same service area. Thus, the spectrum utilization efficiency can be improved while the mutual interference increases. To alleviate the above problems effectively, several new technologies such as multiband [16], double beam [17], and polarization diversity [18] are desirable.

Dual-band antennas [19], [20] are increasingly used to drastically reduce the number of required antennas because they can integrate two operating frequency bands in the same antenna volume. Dual-polarized diversity antennas are used to reduce multipath fading and interference due to their high port-to-port isolation and low cross-polarization level. However, most dual-polarization antennas mainly operate in a single frequency band [21], while dual-band antennas mainly focus on single polarization. Dual-band dual-polarized base station antenna topologies [22] are still rarely reported.

Without loss of generality and for proof-of-concept purposes, we propose in this paper a novel dual-band, miniaturized, and low-profile base station antenna, where the two bands cover 820–960 and 1710–2170 MHz bands at the same time with good miniaturization characteristics as the diameter is only 200 mm. It is a low-profile antenna with a tubular radome, which can reduce the impact on surrounding environments. The proposed antenna can achieve the following advantages in many application scenarios: 1) to solve the difficult problem of site selection; 2) to minimize the impact on surrounding urban environments and the resulting residents' concerns about the health safety of radiated radio waves; and 3) to optimize the network coverage in dense urban areas.

This paper is organized as follows. Section II compares three kinds of design implementation schemes for base station antennas. The simulation of the proposed antenna array is designed in Section III with an experimental verification presented in Section IV. Conclusion is drawn in Section V.

Manuscript received June 22, 2014; revised June 09, 2015; accepted September 07, 2015. Date of publication September 23, 2015; date of current version November 25, 2015. This work was supported in part by the National Natural Science Foundation of China under Grant 61372077, in part by the Fundamental Research Program of Shenzhen City under Grant JC201005250067A and Grant JCJY20120817163755061, and in part by Guangdong Provincial Science and Technology Program under Grant 2013B090200011.

Yejun He, Z. Pan, X. Cheng, Yuan He, and J. Qiao are with Shenzhen Key Laboratory of Antennas and Propagation, College of Information Engineering, Shenzhen University, Shenzhen 518060, China (e-mail: heyejun@126.com; panzz89@126.com; cxd199181@126.com; heyuan0022@126.com; qiaojian1@gmail.com).

M. M. Tentzeris is with the School of Electrical and Computer Engineering, Georgia Institute of Technology, Atlanta, GA 30332 USA (e-mail: etentze@ece.gatech.edu).

Color versions of one or more of the figures in this paper are available online at http://ieeexplore.ieee.org.

Digital Object Identifier 10.1109/TAP.2015.2481488

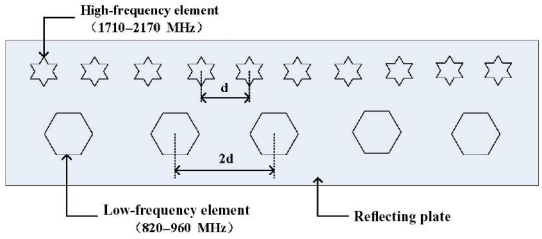

Fig. 1. Side-by-side scheme.

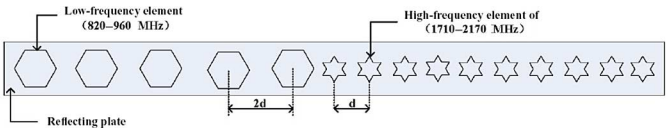

Fig. 2. Up-and-down coaxial scheme.

II. Comparison of Design Implementation Schemes for Base Station Antennas

In terms of different arrangement schemes of radiating elements, base station antennas can be divided into three categories: side-by-side scheme, up-and-down coaxial scheme, and embedded scheme. These schemes are discussed to select the most appropriate one for the proposed antenna.

A. Side-by-Side Scheme

In the side-by-side scheme, the two arrays for the two bands are placed on a reflection plate in parallel, where one raw denotes the high-frequency elements and the other raw represents the low-frequency elements as shown in Fig. 1.

Since the antenna gain is proportional to the number of elements [23], if the required antenna gain in 820–960 MHz band is 15 dBi, then five elements need to be used for the low-frequency subarray. If the antenna gain in 1710–2170 MHz band is 18 dBi, 10 elements need to be used for the high-frequency subarray. However, the spatial distance between the two adjacent antenna subarrays depends on the operating frequency. Because the high-frequency operating frequency in this paper is twice of the low-frequency operating frequency, the spatial distance between adjacent high-frequency elements is a half of that between adjacent low-frequency elements.

However, side-by-side dual-band antenna implementations result in an increased width of the composite antenna array. Furthermore, the far-field radiation pattern is greatly affected as the two-row antenna elements are not placed exactly on the center line of reflecting plate.

B. Up-and-Down Coaxial Scheme

The up-and-down coaxial scheme is designed according to the following two constraints: 1) the right half part consists of high-frequency elements and the left half part consists of low-frequency elements as shown in Fig. 2 and 2) two single-band antennas in different bands are connected up and down, where these elements are placed on a long reflection plate.

The up-and-down coaxial scheme is simpler than the side-by-side scheme because the single frequency base station antennas

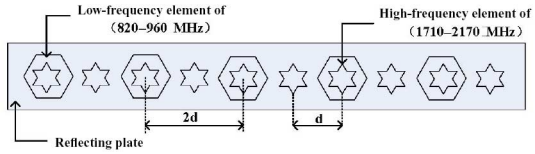

Fig. 3. Embedded scheme.

were developed maturely. This is due to negligible mutual coupling, which does not require the antenna elements to be repositioned. This connecting scheme has no effect on two separate antennas, so it is not necessary to consider the mutual coupling and readjusting the element position after connecting. Furthermore, this scheme can reduce the antenna's design cycle compared to the first scheme.

Since two single antennas are connected into one antenna by up-and-down coaxial scheme, the length of the antenna is sum of the length of the two subarrays. Moreover, the main feed line that is placed in upper part of the antenna needs to access the input signal via the lower part of the antenna, which increases the length of the main feed line greatly. The longer the feed line length is, the greater the losses are. Thus, the gain of the upper elements is effectively less than that of the lower elements.

C. Embedded Scheme

In the embedded scheme as shown in Fig. 3, elements are arranged where a high-frequency element follows a low-frequency element. The distance between two adjacent low-frequency elements is twice as much as that between two adjacent high-frequency elements. Therefore, every second high-frequency element is also embedded in a low-frequency element. The linear array elements are merged into the same space, thus reducing volume.

Compared with the previous two schemes, the embedded scheme features a great advantage in the composite antenna topology size/area resulting in the elimination of the need for increased length or width. Within the same physical size/area of a single-band antenna, this antenna can operate at two bands.

However, the scheme increases the design difficulty because embedded elements operating in different frequency bands increase the parasitic coupling between the high-frequency and low-frequency elements, especially in combined colocated elements requiring a readjustment of the radiation. Thus, the adjusting for the antenna pattern and the isolation are essential. Furthermore, unlike the previous two schemes, this scheme—which is chosen for the proposed antenna—involves effectively novel designs with unique miniaturization characteristics and challenges.

III. Design of Antenna Array

A. Design of Element

When designing the individual radiating elements according to the embedded scheme selected above, we need to consider the following several factors: 1) the mutual coupling between a high-frequency element and a low-frequency element especially for high-frequency elements that are embedded within low-frequency elements; 2) the effect of adjacent elements on

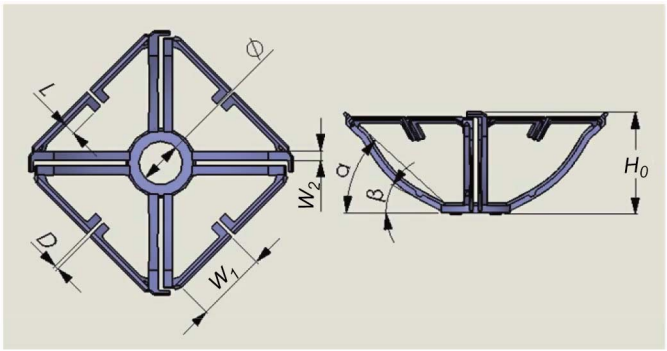

Fig. 4. Low-frequency element (*left*: vertical view and *right*: side view).

the radiation pattern as well as on the interelement coupling; and 3) due to the bandwidth and polarization requirements, every individual radiating element should be broadband and dual-polarized.

1) Low-Frequency Radiation Element: In order to reduce the mutual coupling between the high-frequency and low-frequency radiation elements as much as possible, and have the advantages of a simple low-profile structure, convenient manufacturing, high reliability, and good electrical properties, we chose the low-frequency band to design a square-aperture planar broadband dual-polarization radiating element which looks like a bowl as shown in Fig. 4. It includes two groups of radiation arms, four dipoles which are orthogonal with each other between the two groups, four couples of baluns and a cricoid pedestal (or called base bottom) [24]. In the cricoid pedestal, there are screw holes for convenient installation. The proposed low-frequency radiation element has the following characteristics: 1) the square-mouth diameter is reduced to $0.35-0.45\lambda$ (typically 0.40λ, λ means wavelength) to effectively reduce the mutual coupling between adjacent radiation elements; 2) the four square vertices correspond to the four dipole feed points; 3) the radiation arm of each element is composed of the straight part and the loading part, where the loading part can effectively expand the bandwidth and improve the radiation performance; and 4) at least two pairs of adjacent radiation arms of adjacent dipole are in the same plane, which is tilt relative to the aperture plane. The radiation arms gradually converge to the center of radiation element. This feature can increase the distance between low-frequency elements and the high-frequency elements to obviously reduce the effect of the low-frequency element on the adjacent high-frequency element, especially on the standing wave ratio and the isolation; 5) four couples of baluns' base bottom (or called pedestal) is connected to form a circular base bottom, and the base bottom is provided with screw holes, which are easy to install.

Thus, the radiating element features miniaturization, broadband, low array mutual coupling, good radiation performance, etc., while it has the advantages of a simple structure, simple fabrication, high reliability with a topology that can be easily applied to a variety of single frequency, dual-band, and multiband antennas.

The specific parameters of the individual low-frequency radiation element in Fig. 4 are listed in Table I.

TABLE I
SOME PARAMETERS IN FIGS. 4–6

Fig.	Symbol	Description	Value
4	ϕ	Base bottom diameter	31.5 mm
	L	Loading part of radiation arm	8 mm
	D	Gap between two adjacent loading part	2.7 mm
	W_1	Straight part of radiation arm	51 mm
	W_2	Balun width	6.8 mm
	H_0	Total height of element	74 mm
	α	Upper limit angle	43°
	β	Angle between alpha and horizontal plane	31°
5	W_3	Half dipole width	26 mm
	W_4	Fan-shaped line width	9 mm
	D_1	Distance between two adjacent dipoles	2 mm
	L_1	Length of feed piece	18.4 mm
	L_2	Length of hole on the feed piece	16.4 mm
	R	Radius of holes on feed piece	0.75 mm
	W_5	Thickness of feed piece	1 mm
	W_6	Gap between two feed pieces	1 mm
	H_1	Total length of element	39 mm
6	La	Reflection plate length	740 mm
	Wa	Bottom width of reflection plate	170 mm
	γ	Bevel angle of reflection plate	105°
	l_1	Inclined side of reflection plate	30 mm
	l_2	Folding side of reflection plate	5 mm
	h	Vertical distance between reflection plate bottom surface and cylinder center of cover	15 mm
	a	Length of hypotenuse of surrounding isolation baffle	52 mm
	b	Edge length of surrounding isolation baffle	30 mm
	c	Height of side of surrounding isolation baffle	9 mm
	d	High-frequency element spatial distance	140 mm
	W_b	Distance between low-frequency element center and rectangular baffle	70 mm
	W_c	Width away from array element center	60 mm
	L_b	Length of rectangular baffle	110 mm
	H_2	Height of rectangular baffle	35 mm

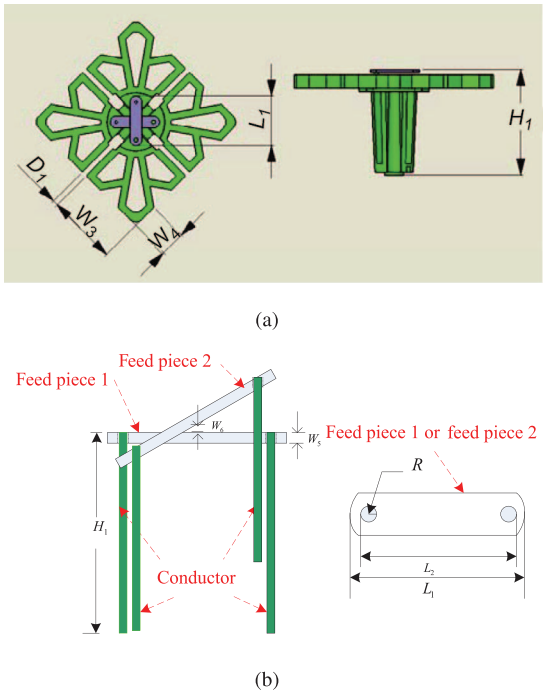

Fig. 5. (a) High-frequency element. *Left*: vertical view and *right*: side view. (b) Feed piece 1 and feed piece 2. *Left*: 3-D view and *right*: top view.

2) High-Frequency Radiation Element: We chose to design a fan-shaped ultra wideband dual-polarized radiating element as shown in Fig. 5. It consists of two dipoles which are orthogonal to each other with balun (balanced–unbalanced) connectors, and the orthogonal arrangement of the "–" feed piece [25]. Each dipole consists of two fan-shaped half dipoles. Feed piece which can feed the dipole by the balanced–unbalanced connector two half dipoles also plays a supporting role to the radiation arm. This design mainly has the following three advantages: 1) The radiation arm is composed of four identical fan-shaped half dipoles symmetrically, where every fan-shaped half dipole adopts a hollow shape to effectively reduce its weight, while the current is flowing mainly on the edges of the radiation arm. The hollow shape results in a minimal effect on the radiation performance. 2) The radiation arm edge adopts a polygon shape and is hollow configuration as illustrated in Fig. 5(a) so as to extend the radiation arm effective length. Extending in this way the current distribution path, not only increases the bandwidth but also reduces the element physical aperture area to enhance its miniaturization. 3) The feed piece adopts a straight structure, which is simple and not easy to deform improving the consistency of standing wave performance compared to commonly utilized a right angle type feed piece structure.

Therefore, the high-frequency radiation elements not only obtain the dual-polarized broadband characteristics but also avoid affecting significantly the low-frequency radiation characteristics. The proposed feeding configuration has the advantages of simple structure, light weight, casting molding and consistency, easy assembly, etc.

The specific parameters of every individual high-frequency radiation element in Fig. 5 are listed in Table I.

B. Antenna Array Model

If the high-frequency gain is 18 dBi and the low-frequency gain is 15 dBi, the number of high-frequency elements is 10, and the number of low-frequency elements is 5. The number of elements mainly influences the gain of the antenna and E-plane pattern. Moreover, the H-plane pattern is often used in simulations, where the beamwidth and the front-to-back ratio (FBR) only depend on the shape of reflection plate regardless of the length of the antenna. For ease of simulations, we only use five-element high-frequency and two-element low-frequency simplified model in accordance with the third scheme—embedded scheme.

Fig. 6(a) shows the antenna array simulation model, which mainly comprises a reflection plate, high-frequency elements, low-frequency elements, rectangular baffles, and surrounding isolation baffles. Reflection plates and baffle plates are made from aluminum. Because the dual-band antenna is heavier than single-band antenna, the thickness of the reflection plate is 2.5 mm and the thickness of the isolation plate is 1 mm. Since, high-frequency and low-frequency elements are embedded in the same axis, the mutual coupling between elements is very large. Thus, we add some frames around elements and optimize the shape and the size of the frame to achieve a decoupling effect. The beamwidth is more converged. The baffle is used to direct the radiation of power density in the desired direction and not on other undesired directions, while it also improves the isolation between elements and the antenna FBR. Because the baffle shape of the reflection plate impacts on the H-plane pattern, the reflection plate needs to be optimized more carefully.

In order to accurately simulate the practical environments, the tubular radome needs to be appended in simulation model as shown in Fig. 6(b) (The outer diameter of the cover is 200 mm; the wall thickness of the cover is 3 mm; the material of the cover is UPVC; and the dielectric constant is 3.8). Fig. 6(c) is an enlarged Fig. 6(a). The optimum size of the proposed antenna in Fig. 6 is shown in Table I.

C. Simulation Results and Analysis

Modeling and simulation of the antenna are difficult since it needs to constantly modify variable parameters, and use different methods to obtain optimized pattern. In the simulation, the antenna size is limited (the diameter is 200 mm). After simulation and optimization for a period of time, some rules are obtained: the width increasing of the reflection plate results in higher FBR and bigger beamwidth in high frequency, and low FBR and beamwidth in low frequency. The length of the inclined side of the reflection plane and the bevel angle changes have little influence on the high-frequency pattern but greatly affect the low-frequency pattern. The surrounding isolation baffle is around the high-frequency element to make the high-frequency beamwidth more converged and increase FBR in the low frequency. As the rectangular baffle increases, the FBR in the high frequency and low frequency will increase, but the beamwidth will become wider. Therefore, the element spatial distance and the antenna height in the outer cover are taken as an example to give a detailed description.

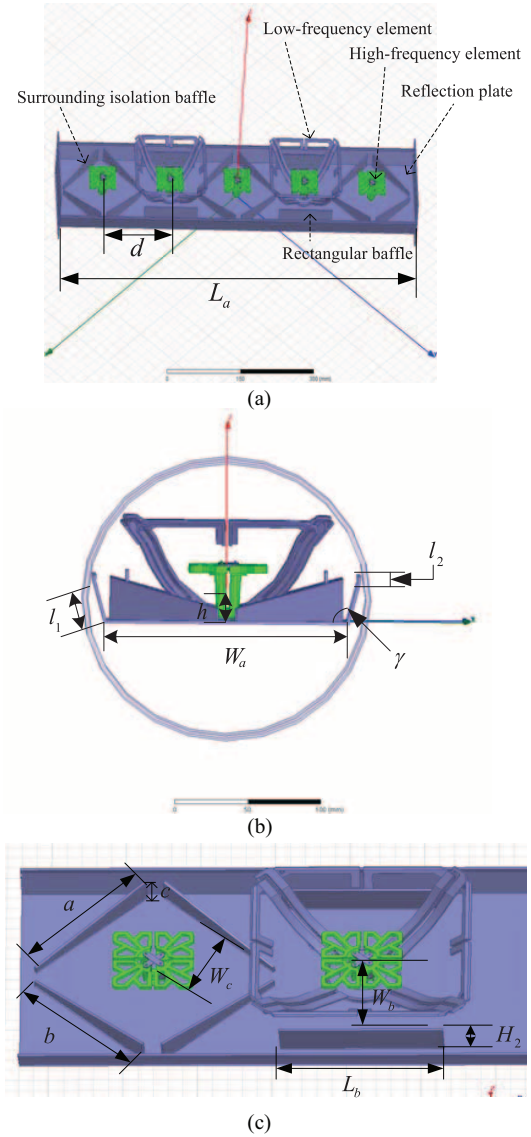

Fig. 6. Simplified antenna array simulation model. (a) High-frequency five-element and low-frequency two-element model. (b) Sectional view. (c) Zoom-in view.

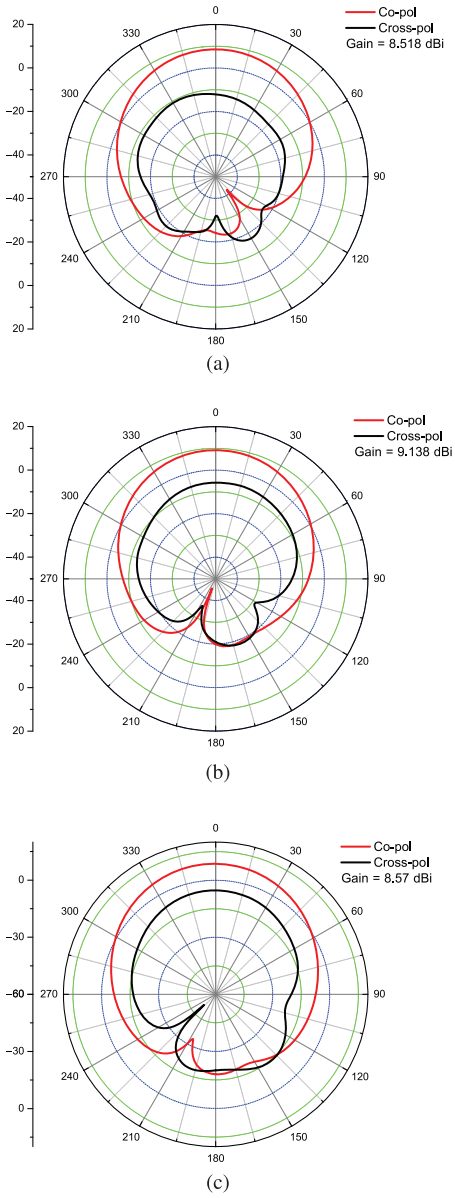

Fig. 7. Simulated H-plane gain patterns for two elements in different spatial distances ($f = 1.894$ GHz). (a) 0.5λ. (b) 0.7λ. (c) λ.

TABLE II
GAIN SIMULATION FOR TWO ELEMENTS IN DIFFERENT ELEMENT SPATIAL DISTANCES

Distance (mm)	0.5λ	0.6λ	0.7λ	0.8λ	0.9λ	1λ
Gain (dBi)	8.518	8.96	9.138	9.037	8.825	8.57

1) Determination of Spatial Distance Between Two Adjacent Elements: Spatial distance between two adjacent elements is an important parameter used in antenna array pattern synthesis. The small element spatial distance makes the effective radiation area overlap. Conversely, the big element spatial distance results in the high sidelobe. Therefore, the choice of a suitable element spatial distance is necessary.

Simulated H-plane gain patterns for two elements in different spatial distances in the frequency band of 1710–2170 MHz are shown in Fig. 7, where $\lambda = 200$ mm. From Fig. 7 and Table II, it can be seen that with the increase of the element spatial distance, the gain of the antenna first slowly increases, then gradually reduces. When the element spatial distance is 0.7λ (140 mm), the gain of the antenna reaches the maximum of 9.138 dBi. Therefore, the high-frequency element spatial distance is set as 140 mm. However, in the dual-band antenna, in addition to considering the high-frequency element spatial distance, the low-frequency element spatial distance also needs to be determined. For the high-frequency range from 1710 to 2170 MHz and the low-frequency range from 820 to 960 MHz, the high-frequency antenna operating frequency is almost twice as much as the low-frequency antenna operating frequency. The high-frequency element wavelength is half of the low-frequency element wavelength, therefore the low-frequency element spatial distance is 280 mm.

2) Antenna Height in the Cover: In the simulation process of the low-profile antenna proposed in this paper, we need to optimize the height of the antenna body h in the cover as shown

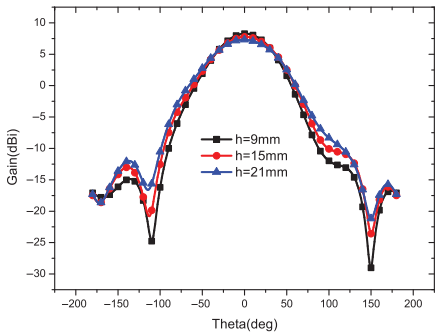

Fig. 8. Simulated H-plane gain patterns operating in high frequency with different heights h ($f = 1.894$ GHz).

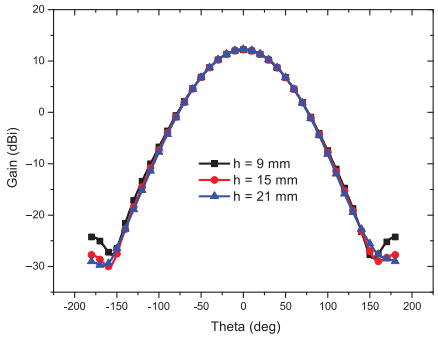

Fig. 9. Simulated H-plane gain patterns operating in low frequency with different heights h ($f = 880$ MHz).

in Fig. 6(b), where the height of the antenna body in a cover is defined as the vertical distance between the reflection plate bottom surface and the cylinder center of the cover. In the planar antenna, the height of antenna body is fixed. However, in the cover of low-profile antenna, although the width of the antenna is limited, the upper and lower space is allowed to adjust. Therefore, the height of the antenna body in a cover will affect the pattern performance. A detailed analysis and simulation for this parameter is done, where initial value of h is set as 0. If the antenna array moves up, h is positive; otherwise, h is negative. When the antenna array moves down, the high-frequency and low-frequency patterns get worse. Thus, we only analyze the effect of the antenna body moving up on the pattern. Simulated gain patterns in high frequency and low frequency are shown in Figs. 8 and Fig. 9, respectively.

Simulated H-plane gain patterns operating in high frequency with different heights are shown in Fig. 8, where the antenna gain reduces and the beamwidth and the FBR increase with increasing of the height. In other words, in high frequencies, the antenna array moving up results in a worse pattern. Simulated H-plane gain patterns operating in low frequency with different heights are shown in Fig. 9. With the increasing of the height, the FBR also increases, but the gain and the beamwidth are essentially unchanged. Therefore, in low frequency, the antenna array moving up results in a better pattern. With the change of the height, high-frequency and low-frequency pattern changes are contradicted. The tradeoff height between the above two is $h = 15$ mm.

3) Optimized Simulation Results: According to the conclusion drawn in the simulation, the reflection plate size and the isolation baffle size are further optimized as shown in Table I. Based on these sizes, simulated H-plane gain patterns are obtained as shown in Fig. 12(a)–(d), where all cross-polarization levels are lower than copolarization levels in main direction, and the low-frequency simulation pattern curves are smooth and the high-frequency simulation pattern curves fluctuate obviously. The reason why the high-frequency simulation pattern curves fluctuate is that a high-frequency element is embedded in a low-frequency element which results in a big mutual coupling effect. Nonetheless, the high-frequency and low-frequency FBRs are basically larger than 25 dB, the beamwidth is converged and the cross-polarization ratio for main direction is larger than 10 dB. The only disadvantage is that cross-polarization ratio for $\pm 60^\circ$ from main direction is not ideal in high frequency, which can be improved in the practical antenna adjusting.

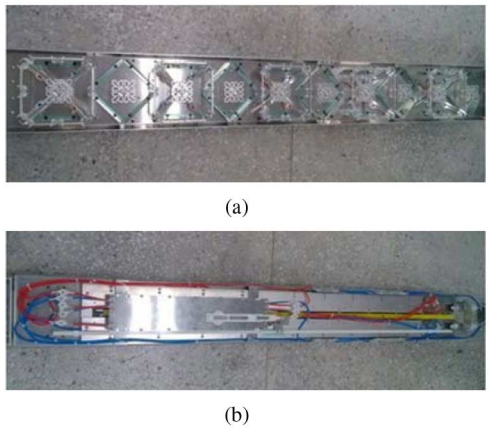

(a)

(b)

Fig. 10. Prototype of dual-band miniaturized low-profile base station antenna array. (a) Front view. (b) Back view.

IV. Measured Results and Verification

A. Antenna Prototype

According to the optimum size and the gain requirement in the simulation, a dual-band array with 5 low-frequency elements and 10 high-frequency elements is fabricated. A dual-band miniaturized base station antenna array is shown in Fig. 10, where the front view of the antenna is the radiation element and the back view of the antenna is the feed network. The practical antenna array size is the extension of the simulation model in Fig. 6. The practical length of the antenna array is 1500 mm and the width of the antenna array is 170 mm.

B. Performance Analysis

Due to the differences between the realistic environment and simulation environment, and the errors of the fabricating and assembly, the measured results are not as good as the simulation results. Thus, we should adjust the antenna in the practical environment to obtain the optimal measured results. For example, the isolation in the high-frequency band is adjusted by appending an isolation baffle beside the third high-frequency element and appending a linear-shape isolation baffle beside the second, third, and fifth high-frequency element; the isolation

in low-frequency band is adjusted by appending a long isolation bar through reflection plate beside the first low-frequency element.

The measured results on S parameters and $+45^\circ$ polarization patterns are shown in Figs. 11–13. -45° polarization patterns are omitted due to symmetry. Fig. 11(a)–(d) shows not only measured VSWR and measured isolation (S_{21}) but also simulated VSWR and simulated isolation (S_{21}). In simulated VSWR results, the maximum VSWR in the high frequency is 1.5; the VSWR in the low frequency is very ideal and the VSWR curves in two ports in the low frequency are similar, which illustrate the VSWR consistency performs well. In the practical antenna adjusting, we also need to further enhance this parameter. In measured VSWR results, the VSWR in high frequency and the VSWR in low frequency are less than 1.3, which meets the design requirements. In simulated isolation (S_{21}) results, the maximum value of the high-frequency isolation (S_{21}) is -30 dB, which meets the requirements. Isolation in low frequency is better, which illustrates a small mutual coupling effect between two ports in low frequency. In the practical antenna adjusting, we also need enhance the isolation. In measured isolation (S_{21}) results, the isolation in the high-frequency band is greater than 30 dB and the isolation in the low frequency band is greater than 33 dB, which all meet the requirement that the isolation should be greater than 30 dB.

Fig. 12(a)–(d) also shows measured H-plane gain patterns, where the gain in the high frequency is 18 ± 1 dBi and the gain in the low frequency is 14 ± 1 dBi, which are all in the allowed range. From Fig. 12, we can see the FBR is larger than 25 dB and the beamwidth is convergent. In the range of $65 \pm 6^\circ$, the cross-polarization ratio for main direction is greater than 15 dB. The cross-polarization ratios for $\pm 60^\circ$ from main direction are less than 10 dB in individual points in high frequency, but it does not impact on the antenna's operation. The measured results are in good agreement with the simulated results.

Measured H-plane and E-plane gain patterns are simultaneously shown in Fig. 13(a)–(d). In measured E-plane gain patterns, the first sidelobe level in high frequency is slightly higher, but the difference relative to the main lobe is over 15 dB, which meets the design requirements. It is very clear that the low-frequency pattern is good. In short, from these measured results, the electrical performance is quite good.

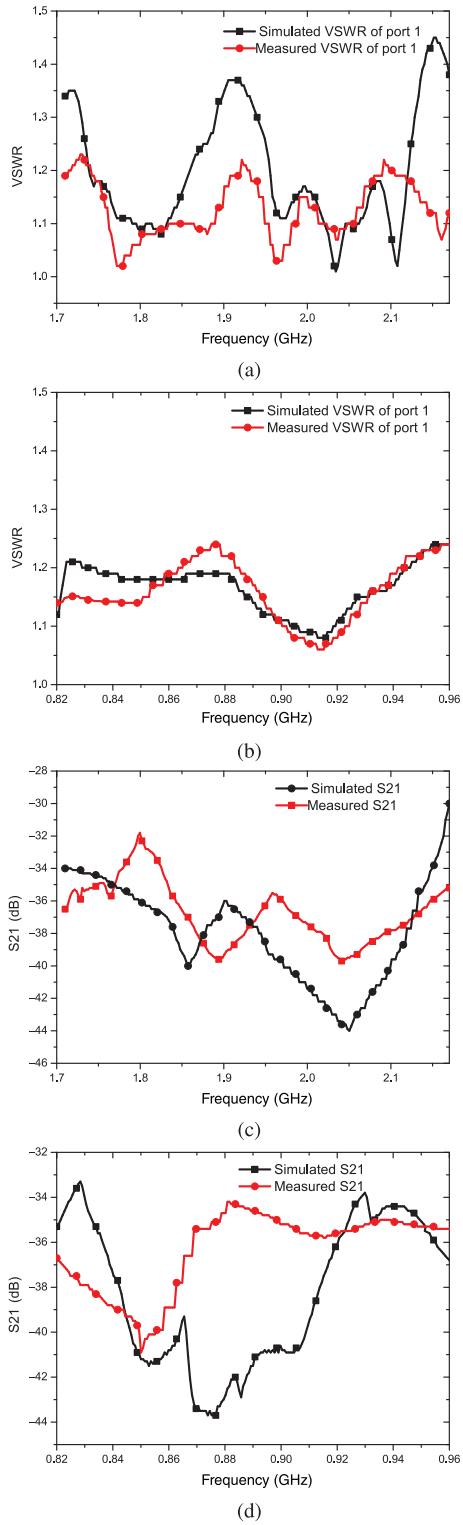

Fig. 11. (a) Voltage standing wave ratio (VSWR) in high frequency. (b) VSWR in low frequency. (c) Isolation (S_{21}) in high frequency. (d) Isolation (S_{21}) in low frequency.

C. Comparative Analysis

In order to demonstrate the advantages of the designed antenna, we compare the designed antenna with the antenna proposed in [26]. The two antennas operate in the same band, i.e., the low frequency band is 820–960 MHz and high-frequency band is 1.71–2.17 GHz; they have the same number of the elements and the similar innerconstruct which are all embedded. In contrast to the ordinary plate cover in [26], we select the low-profile tubular radome. The following comparison mainly consists of three factors: volume, performance, and appearance.

1) Volume Comparison: The reflector width of the commonly utilized antenna under comparison is 240 mm, while the reflector width of antenna proposed in this paper is 185 mm. Because the array element spatial distance is the same, the total physical length of both antennas is the same. From the comparison, it can be seen that the volume of the proposed antenna is significantly reduced and the design target of miniaturization is achieved.

2) Performance Comparison: The highest gain of the antenna designed in this paper is 13.8 dBi in the low frequency

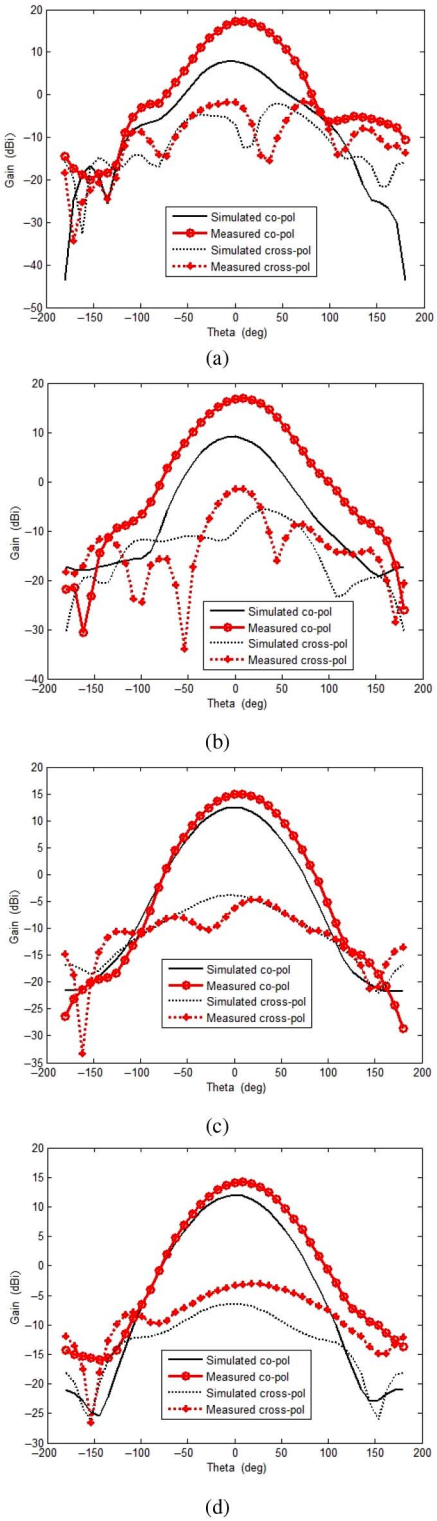

Fig. 12. Simulated and measured H-plane gain patterns in (a) high frequency of 2.17 GHz, (b) high frequency of 1.71 GHz, (c) low frequency of 0.96 GHz, and (d) low frequency of 0.824 GHz.

and 16.7 dBi in the high frequency. The highest gain of the comparative antenna is 13.4 dBi in the low frequency and 15.6 dBi in the high frequency. The minimum FBR in this paper is 24.1 dB, and the minimum FBR in the comparative antenna is 23.1 dB.

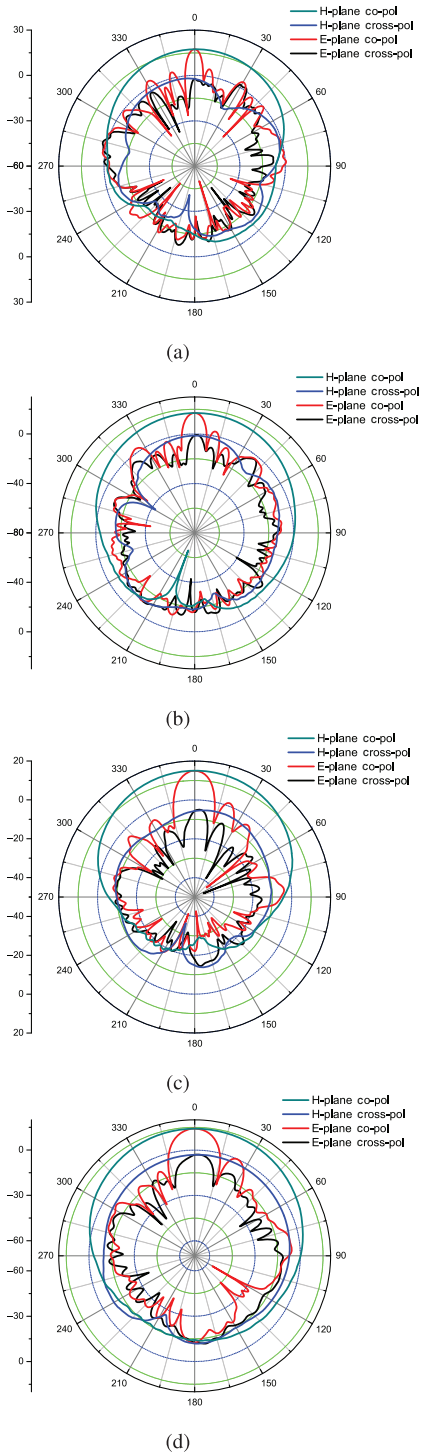

Fig. 13. Measured H-plane and E-plane gain patterns in (a) high frequency of 2.17 GHz, (b) high frequency of 1.71 GHz, (c) low frequency of 0.96 GHz, and (d) low frequency of 0.824 GHz.

3) Appearance Comparison: This paper uses a tubular form of radome, which is different from the ordinary plate cover. The low-profile antenna with a tubular form of radome has a special appearance so that the antenna has a certain appearance and concealment. Fig. 14 shows two typical application scenarios for the proposed low-profile base station antenna and an ordinary plate base station antenna. From this

(a) (b)

Fig. 14. Application example for the (a) proposed base station antenna and (b) ordinary plate base station antenna, respectively.

figure, we can see that the low-profile antenna can be easily installed in a minimum environmental impact configuration.

From the comparison of the previous three aspects, we find the dual-band, miniaturized, low-profile base station antenna designed in this paper not only operates in a wideband but also has some advantages such as small size, high gain, characteristics of concealment and easy installation. From the analysis of market demands, the proposed antenna is a valuable scheme to meet the commercial requirements.

V. Conclusion

In order to meet the increasing traffic demands of cellular communication networks, a novel dual-band, dual-polarized, miniaturized and low-profile base station antenna was proposed in this paper. This antenna has several advantages: compared with the conventional dual-band planar antennas, the proposed antenna features a reduced volume allowing for miniaturized tubular-form radomes to be placed around it thus minimizing its environmental impact. The proposed dual-band low-profile base station antenna which utilizes the embedded element implementation schemes can be easily applied to commonly used 2G/3G systems meeting the miniaturization requirements without a significant degradation of its radiation performance. In addition, the embedded element arrangement in this paper can also be transplanted to 4G/5G base station antenna design.

References

[1] C. L. Lin, *Antenna Engineering Handbook*. Beijing, China: Publishing House of Electronics Industry, 2002.

[2] J. D. Kraus, *Antennas: For All Applications*. Beijing, China: Publishing House of Electronics Industry, 2005.

[3] C. A. Balanis, *Antenna Theory Analysis and Design*. Hoboken, NJ, USA: Wiley, 2005.

[4] J. A. Kong, *Electromagnetic Wave Theory*. Beijing, China: Publishing House of Electronics Industry, 2003.

[5] J. Qiao, X. Shen, J. W. Mark, Q. Shen, Y. He, and L. Lei, "Enabling device-to-device communication in millimeter wave 5G cellular networks," *IEEE Commun. Mag.*, vol. 53, no. 1, pp. 209–215, Jan. 2015.

[6] P. Strickland and F. Bacchus, "Microstrip base station antennas for cellular communications," in *Proc. 41st IEEE Veh. Technol. Conf.*, 1991, pp. 166–171.

[7] W. Sadowski and C. Peixeiro, "Microstrip patch antenna for a GSM 1800 base station," in *Proc. 12th Int. Conf. Microw. Radar*, 1998, pp. 409–413.

[8] N. Herscovici and C. Christodoulou, "Potentials of smart antennas in CDMA systems and uplink improvements," *IEEE Antennas Propag. Mag.*, vol. 43, no. 5, pp. 172–177, Oct. 2001.

[9] Y. He, X. Hou, J. Huang, and F. C. M. Lau, "Simulation and implementation of dual-polarization TD-SCDMA smart antennas," in *Proc. 15th Asia-Pac. Conf. Commun. (APCC'09)*, 2009, pp. 217–220.

[10] S. Finistauri, G. Marrocco, G. D'Orio, M. Motta, and S. De Polo, "Investigation on pattern distortion of landscape-compliant 3G base-station antennas," in *Proc. IEEE Antennas Propag. Soc. Int. Symp.*, 2004, vol. 1, pp. 1054–1057.

[11] K.-M. Luk and B. Wu, "The magnetoelectric dipole—A wideband antenna for base stations in mobile communications," *Proc. IEEE*, vol. 100, no. 7, pp. 2297–2307, Jul. 2012.

[12] M. A. Soliman, W. Swelam, A. Gomaa, and T. E. Taha, "Steerable dual-band planar microstrip phased array antenna for 3G and 4G wireless communication systems," in *Proc. IEEE-APS Topical Conf. Antennas Propag. Wireless Commun. (APWC)*, 2001, pp. 905–908.

[13] W. An, H. Wong, K. L. Lau, S. Li, and Q. Xue, "Design of broad-band dual-band dipole for base station antenna," *IEEE Trans. Antennas Propag.*, vol. 60, no. 3, pp. 1592–1595, Mar. 2012.

[14] Y. Cui, R. Li, and P. Wang, "A novel broadband planar antenna for 2G/3G/LTE base stations," *IEEE Trans. Antennas Propag.*, vol. 61, no. 5, pp. 2767–2774, May 2013.

[15] Y. Cui, R. Li, and P. Wang, "Novel dual-broadband planar antenna and its array for 2G/3G/LTE base stations," *IEEE Trans. Antennas Propag.*, vol. 61, no. 3, pp. 1132–1139, Mar. 2013.

[16] Y. Yamada, and M. Kijima, "A slender two beam base station antenna for mobile radio," in *Proc. IEEE Antennas Propag. Soc. Int. Symp.*, 1994 vol. 1, pp. 352–355.

[17] P. Raumonen, L. Sydanheimo, L. Ukkonen, M. Keskilammi, and M. Kivikoski, "Folded dipole antenna near metal plate," in *Proc. IEEE Antennas Propag. Soc. Int. Symp.*, 2003, vol. 1, pp. 848–851.

[18] R. G. Vaughan, "Polarization diversity in mobile communications," *IEEE Trans. Veh. Technol.*, vol. 39, no. 3, pp. 177–186, Aug. 1990.

[19] L. Siu, H. Wong, and K. M. Luk, "A dual-polarized magnetoelectric dipole with dielectric loading," *IEEE Trans. Antennas Propag.*, vol. 57, no. 3, pp. 616–623, Mar. 2009.

[20] V. Erceg, P. Soma, D. S. Baum, and S. Catreux, "Multiple-input multiple-output fixed wireless radio channel measurements and modeling using dual-polarized antennas at 2.5 GHz," *IEEE Trans. Wireless Commun.*, vol. 3, no. 6, pp. 2288–2298, Nov. 2004.

[21] S. Karimkashi and G. Zhang, "A dual-polarized series-fed microstrip antenna array with very high polarization purity for weather measurements," *IEEE Trans. Antennas Propag.*, vol. 61, no. 10, pp. 5315–5319, Oct. 2013.

[22] N. I. M. Elamin, T. A. Rahman, and A. Y. Abdulrahman, "New adjustable slot meander patch antenna for 4G handheld devices," *IEEE Antennas Wireless Propag. Lett.*, vol. 12, pp. 1077–1080, Sep. 2013.

[23] M. T. Ivrla and J. A. Nossek, "Receive antenna gain of uniform linear arrays of isotrops," in *Proc. IEEE Int. Conf. Commun.*, 2009, pp. 1–6.

[24] Q. Liu *et al.*, "Wideband dual polarized radiating element and antenna," Chinese Patent CN103094668A, May 8, 2013.

[25] S. Luo *et al.*, "Ultra wideband dual polarized radiating element and array antenna," Chinese Patent CN103151603A, Jun. 12, 2013.

[26] Z. K. Pan, "*The design of the dual-band antenna and dual-polarized base station antenna*," M.S. thesis, School Elect. Inform., South China Univ. Technol., Guangzhou, China, 2012.

Yejun He (SM'09) received the B.S. degree in mechatronics engineering from Huazhong University of Science and Technology, Wuhan, China, the M.S. degree in communication and information system from Wuhan University of Technology (WHUT), Wuhan, China, and the Ph.D. degree in information and communication engineering from Huazhong University of Science and Technology (HUST), Wuhan, China, in 1994, 2002, and 2005, respectively.

From September 2005 to March 2006, he was a Research Associate with the Department of Electronic and Information Engineering, Hong Kong Polytechnic University,

Hong Kong. From April 2006 to March 2007, he was a Research Associate with the Department of Electronic Engineering, Faculty of Engineering, Chinese University of Hong Kong, Hong Kong. From July 2012 to August 2012, he was a Visiting Professor at the Department of Electrical and Computer Engineering, University of Waterloo, Waterloo, ON, Canada. From October 2013 to October 2015, he was an Advanced Visiting Scholar (Visiting Professor) at School of Electrical and Computer Engineering, Georgia Institute of Technology, Atlanta, GA, USA. He is currently a Full Professor with Shenzhen University, Shenzhen, China and the Director of Shenzhen Key Laboratory of Antennas and Propagation, Shenzhen University. He has authored or coauthored more than 90 research papers, books (chapters) as well as obtained over 12 authorized patents. His research interests include channel coding and modulation, MIMO-OFDM wireless communication, space-time processing, antennas and propagation, and so on.

Dr. He is an Associate Editor of the *Security and Communication Networks* journal. He is a Senior Member (SM'07) of China Institute of Communications and a Senior Member (SM'11) of China Institute of Electronics. He is TPC Co-Chair of WOCC 2015. He has served as a Reviewer for various journals such as the IEEE TRANSACTIONS ON VEHICULAR TECHNOLOGY, the IEEE TRANSACTIONS ON COMMUNICATIONS, the IEEE TRANSACTIONS ON INDUSTRIAL ELECTRONICS, the IEEE WIRELESS COMMUNICATIONS, the IEEE COMMUNICATIONS LETTERS, *International Journal of Communication Systems*, *Wireless Communications and Mobile Computing*, and *Wireless Personal Communications*. He has also served as a Technical Program Committee Member or a Session Chair for various conferences, including the IEEE Global Telecommunications Conference, the IEEE International Conference on Communications, the IEEE Wireless Communication Networking Conference, and the IEEE Vehicular Technology Conference. He served as an Organizing Committee Vice Chair of International Conference on Communications and Mobile Computing (CMC 2010) and an Editor of CMC2010 Proceedings. He acted as the Publicity Chair of several international conferences such as the IEEE PIMRC 2012. He is the Principal Investigator for more than 10 current or finished research projects including NSFC of China, the Integration Project of Production Teaching and Research by Guangdong Province and Ministry of Education as well as the Science and Technology Program of Shenzhen City, and so on.

Zhengzheng Pan received the B.S. degree in measurement-control technology and instrumentation from the University of South China, Hengyang, China, and the M.S. degree in electrical and communication engineering from Shenzhen University, Shenzhen, China, in 2011 and 2014.

Her research interests include base station antenna, RFID tag antenna.

Ms. Pan was the recipient of the National Scholarship for Graduate Students in 2013.

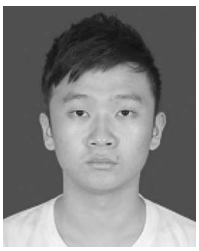

Xudong Cheng received the B.S. degree in communication engineering from Shenzhen University, Shenzhen, China, in 2013. He is currently pursuing the Ph.D. degree in information and communication engineering at the College of Information Engineering, Shenzhen University.

His research interests include channel modeling, especially polarized MIMO channel modeling, energy harvesting communications, smart antennas, and signal processing.

Mr. Cheng was the recipient of the National Scholarship for Graduate Students in 2015.

Yuan He received the B.S. degree in communication engineering from Hunan University of Technology, Zhuzhou, China, and the M.S. degree in electrical and communication engineering from Shenzhen University, Shenzhen, China, in 2012 and 2015, respectively.

His research interests include base station antenna, RFID tag antenna, and radio-frequency circuit.

Jian Qiao received the B.E. degree in electronic information engineering from Beijing University of Posts and Telecommunications, Beijing, China, in 2006, and the Ph.D. and M.A.Sc. degrees in electrical and computer engineering, University of Waterloo, Waterloo, ON, Canada, in 2015, and 2010, respectively.

He is a Postdoctoral Research Fellow with Shenzhen University, Shenzhen, China. His research interests include millimeter wave communication, medium access control, resource management, 5G cellular networks, and mobile video streaming.

Manos M. Tentzeris (S'89–M'92–SM'03–F'10) received the Diploma degree (*magna cum laude*) in electrical and computer engineering from the National Technical University of Athens, Athens, Greece, in 1992 and the M.S. and Ph.D. degrees in electrical engineering and computer science from the University of Michigan, Ann Arbor, MI, USA, in 1993 and 1998, respectively.

He is currently a Professor at the School of Electrical and Computer Engineering, Georgia Institute of Technology, GA, USA. He has served as the Head of the GT-ECE Electromagnetics Technical Interest Group, as the Georgia Electronic Design Center Associate Director for RFID/Sensors research and as the Georgia Tech NSF-Packaging Research Center Associate Director for RF Research and the RF Alliance Leader. He was a Visiting Professor at the Technical University of Munich, Munich, Germany, for the summer 2002, the GTRI-Ireland, Athlone, Ireland, for the summer 2009, LAAS-CNRS, Toulouse, France, for the summer 2010. He has given more than 100 invited talks to various universities and companies all over the world. He has authored more than 580 papers in refereed journals and conference proceedings, 5 books, and 21 book chapters.

Dr. Tentzeris was the TPC Chair for the IEEE IMS 2008 Symposium and the Chair of the 2005 IEEE CEM-TD Workshop and he is the Vice-Chair of the RF Technical Committee (TC16) of the IEEE CPMT Society. He is the Founder and Chair of the RFID Technical Committee (TC24) of the IEEE MTT Society and the Secretary/Treasurer of the IEEE C-RFID. He is the Associate Editor of the IEEE TRANSACTIONS ON MICROWAVE THEORY AND TECHNIQUES and the IEEE TRANSACTIONS ON ADVANCED PACKAGING AND INTERNATIONAL JOURNAL ON ANTENNAS AND PROPAGATION. He is a member of URSI-Commission D, MTT-15 committee, and Technical Chamber of Greece, an Associate Member of EuMA, a Fellow of the Electromagnetic Academy. He served as one of the IEEE MTT-S Distinguished Microwave Lecturers from 2010 to 2012 and is one of the IEEE CRFID Distinguished Lecturers. He was the recipient/corecipient of the 2015 IET Microwaves, Antennas, and Propagation Premium Award, the 2014 Georgia Tech ECE Distinguished Faculty Achievement Award, the 2014 IEEE RFID-TA Best Student Paper Award, the 2013 IET Microwaves, Antennas, and Propagation Premium Award, the 2012 FiDiPro Award in Finland, the iCMG Architecture Award of Excellence, the 2010 IEEE Antennas and Propagation Society Piergiorgio L. E. Uslenghi Letters Prize Paper Award, the 2011 International Workshop on Structural Health Monitoring Best Student Paper Award, the 2010 Georgia Tech Senior Faculty Outstanding Undergraduate Research Mentor Award, the 2009 IEEE Transactions on Components and Packaging Technologies Best Paper Award, the 2009 E.T.S. Walton Award from the Irish Science Foundation, the 2007 IEEE APS Symposium Best Student Paper Award, the 2007 IEEE IMS Third Best Student Paper Award, the 2007 ISAP 2007 Poster Presentation Award, the 2006 IEEE MTT Outstanding Young Engineer Award, the 2006 Asian-Pacific Microwave Conference Award, the 2004 IEEE Transactions on Advanced Packaging Commendable Paper Award, the 2003 NASA Godfrey "Art" Anzic Collaborative Distinguished Publication Award, the 2003 IBC International Educator of the Year Award, the 2003 IEEE CPMT Outstanding Young Engineer Award, the 2002 International Conference on Microwave and Millimeter-Wave Technology Best Paper Award (Beijing, China), the 2002 Georgia Tech-ECE Outstanding Junior Faculty Award, the 2001 ACES Conference Best Paper Award, the 2000 NSF CAREER Award, and the 1997 Best Paper Award of the International Hybrid Microelectronics and Packaging Society.